

Chemistry

Special Topic: Artificial Intelligence and Energy Revolution

Experimental and data-driven investigation of hydrophilic and hydrophobic ionic liquids for supercapacitors

Qiutong Chen, Jifeng Wang & Ying Wang*

*State Key Laboratory of Molecular Engineering of Polymers, Department of Macromolecular Science, Fudan University, Shanghai 200438, China**Corresponding author (email: wying@fudan.edu.cn)

Received 13 June 2025; Revised 27 August 2025; Accepted 14 September 2025; Published online 19 September 2025

Abstract: Ionic liquids (ILs) are promising electrolytes of supercapacitors for high voltage tolerance, zero vapor pressure, excellent thermal stability and environmental friendliness. However, the high viscosity and low ion mobility of ILs limit the capacitance and high-rate performance of the devices. Rather than relying on black-box predictions and screening of advanced ILs for supercapacitors, machine learning models informed by experimentally derived physicochemical parameters can achieve significantly higher accuracy and relevance. According to the comprehensive experimental and data-driven investigation based on electrochemical characterization, nuclear magnetic resonance (NMR) dynamics, quantum and molecular dynamics simulations, we reveal an effective boosting of the specific capacity based on the water solvation mechanism in hydrophilic ILs. We then apply chemistry-informed machine learning to inverse screening and design ILs for supercapacitors based on the critical experimental parameters and morgan fingerprints. These findings elucidate the efficiency and mutual reinforcement of experimental and data-driven investigations in discovering promising materials for energy storage and conversion devices.

Keywords: ionic liquids, supercapacitors, hydrophilicity, water associations, data-driven

INTRODUCTION

Compared with traditional batteries, supercapacitors exhibit unique advantages in terms of high power density and fast response, especially in applications that require instant high power output [1]. Ionic liquids (ILs) are ideal high-voltage electrolytes characterized with zero vapor pressure, excellent thermal stability and environmentally friendly for applications in supercapacitors [2,3]. However, the high viscosity and low ion mobility of ILs constrain the capacitance as applied in supercapacitors [4]. To accelerate the discovery of advanced IL electrolytes for supercapacitors, data-driven methods provide a highly efficient approach when guided by deep chemical insights [5–7]. Rather than relying on black-box predictions, machine learning models informed by experimentally derived physicochemical parameters can achieve significantly higher accuracy and relevance [8,9]. Recent studies have shown that machine learning models built on chemically meaningful descriptors can serve as effective tools. Manna *et al.* [10] integrated molecular dynamics simulations with kernel ridge regression to predict electrochemical windows (ECWs) of ILs for dual-ion

batteries. Descriptors such as ion-pair coordination, diffusion coefficients, and solvation structures are used as model inputs. Yang *et al.* [11] applied interpretable ML to identify key descriptors of reductive stability in lithium battery electrolytes. Building on this, Gao *et al.* [12] showed that Li-solvent coordination tends to lower LUMO (lowest unoccupied molecular orbital) levels and highlighted dipole moment and molecular size as critical features for solvent screening. These examples underscore the value of ML frameworks in rational electrolyte design for energy storage devices.

As the core performance indicator, specific capacitance is closely related to the ion mobility and the interfacial behavior between the electrodes and electrolytes [13]. In the design of supercapacitors, the choice of IL electrolytes determines the operating voltage, the adsorption and desorption rates of ions at the electrodes, and ultimately the specific capacitance [14–16]. Recent research has focused on modifying the structure of ILs or developing IL-based composites with polymers [17,18], redox additives [19,20], organic solvents [21] and nanoparticles [22]. As an environmentally friendly additive, water has proven to be effective in enhancing the performance of ILs [23,24]. The addition of water can promote ion dissociation in ILs [25–27]. When the water content is moderate, it can enhance the ion mobility of the IL, but excessive water may lead to a reduction in the ECW of the electrolyte [28–30]. This “threshold effect” illustrates the importance of water content to the ion dynamics in ILs [31,32].

Despite these experimental and theoretical studies, several key issues regarding the interaction between water and ILs and their correlation with the specific capacitance of supercapacitors remain to be explored. For example: (1) how the specific capacitance evolves in ILs with varying hydrophilicity and water contents; (2) what are the ion associations and mechanisms of water effects on the hydrophilic and hydrophobic ILs; (3) how to quickly target promising ILs to achieve the optimal balance between ECW, conductivity, and specific capacitance. To address these issues, we design a comprehensive experimental investigation of the supercapacitors with commercial activated carbon electrodes based on five ILs with varying hydrophilicity. In addition, through comprehensive nuclear magnetic resonance (NMR) dynamics, quantum calculations, molecular dynamics simulations and machine learning-assisted screening, we reveal an intrinsic relationship between the specific capacitance performance and the critical properties of ILs, such as ion mobility, hydrophilicity, and electrochemical stability. This work enables an experimental and data-driven investigation of the water effects and microscopic dynamics in the ILs for screening potential ILs in supercapacitors, as illustrated in the workflow shown in Figure 1. Moreover, by combining molecular fingerprints and machine learning, we identify the structural determinants of conductivity in ILs, providing insights for the rational design of high-performance ILs. This integration of AI with materials chemistry provides a data-driven framework to efficiently screen, rank, and design IL electrolytes with tailored electrochemical performance for next-generation energy storage systems.

MATERIALS AND METHODS

Materials

1-Ethyl-3-methylimidazolium trifluoromethanesulfonate ([C₂mim][TFO], ≥99%) and 1-ethyl-3-methylimidazolium tetrafluoroborate ([C₂mim][BF₄], electronic grade) were purchased from Proionic. 1-Ethyl-3-methylimidazolium bis(fluorosulfonyl)imide ([C₂mim][FSI], 99.5%) was purchased from Solvionic.

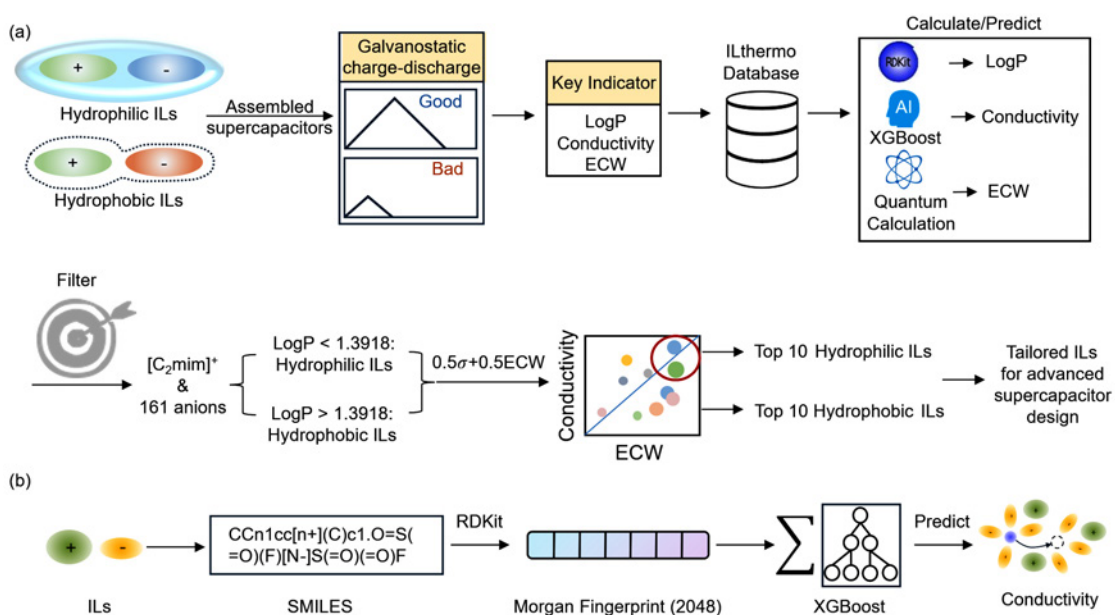


Figure 1 (a) Workflow from experimental analysis to data-driven IL electrolyte design for supercapacitors; (b) XGBoost-based workflow for the prediction of IL conductivity.

1-Ethyl-3-methylimidazolium dicyanofomate ([C₂mim][DCA], RG) and 1-ethyl-3-methylimidazolium bis(trifluoromethylsulfonyl)imide ([C₂mim][TFSI], RG) were purchased from Adamas. Potassium hydroxide (KOH, RG) was purchased from Greagent. Glass microfiber filters (1823-090) were purchased from Whatman. Activated carbon electrode sheets (average loading of 1.38 mg/cm²) were purchased from Shanghai Yanwen Research and Development Technology Co.

Preparation of supercapacitors based on ILs

All pure ILs and activated carbon electrode sheets were baked under vacuum at 80 °C for 24 h. Subsequently, a series of gradient solutions with 1 mL IL and different water contents (0, 1, 2, 3, 4, 5, 10, 50 and 100 μL) were prepared, and the corresponding CR2032 snap-on capacitors with activated carbon electrodes were assembled. Supercapacitors based on pure ILs were assembled in the glovebox (O₂, H₂O < 0.01 ppm), and those with water-containing ILs were assembled in the ambient environment.

Electrochemical tests

Galvanostatic charge-discharge (GCD): The constant current charging and discharging performance of the supercapacitors under different current densities (0.1, 0.2, 0.4, 0.8, 1.6 and 3.2 A/g) were tested by Xinwei test system at room temperature, and all GCD experiments were repeated twice to ensure the accuracy, and the electrode specific capacitance was calculated by the following formula:

$$C_{\text{electrode}} = 2 * \frac{i\Delta t}{mV}, \quad (1)$$

where i is the discharge current in the GCD curve, Δt is the discharge time, V is the voltage window, and m is

the mass of the activated carbon electrode with a mass loading of 1.38 mg/cm².

Characterizations

Nuclear magnetic resonance (NMR)

¹H and ¹⁹F NMR experiments were performed on a 400 MHz Fourier transform NMR spectrometer of a Bruker AVANCE III HD, and peak position and peak area integrations were performed to determine solvation environments and water content. Pulsed field gradient NMR spectroscopy (PFG-NMR) experiments [33] were performed on the cations, anions and water of the electrolytes and fitted to derive diffusion coefficients for each component with the following Stejskal-Tanner equation:

$$I = I_0 e^{-D\gamma^2 g^2 \delta^2 \left(\Delta - \frac{\delta}{3} \right)} \quad (2)$$

where I and I_0 refer to the spin-echo signal intensity and spin-echo signal intensity at zero gradient, respectively. γ is the gyromagnetic ratio of the nucleus, g is the gradient strength, δ is the pulse duration time and Δ is the diffusion time. The diffusion coefficient (D) of a desired nucleus can be obtained by fitting the experimental I vs. g data using Stejskal-Tanner equation. The gradient pulse duration δ was 1–5 ms, diffusion time Δ was 100–1000 ms. The number of scans for each step was adjusted from 2 to 64 to ensure a good signal-to-noise ratio (SNR). Sixteen gradient steps were applied for each diffusion experiment, and the maximum gradient strength was selected to achieve $\geq 90\%$ NMR signal attenuation.

Conductivity test

The Orion Star A212 conductivity meter was calibrated at room temperature using a 1413 $\mu\text{S}/\text{cm}$ standard, and then the conductivity of each mixture was tested individually with three repetitions. The standard deviation was in the range from 0.0015 to 0.19 mS/cm.

Computational methods

Quantum chemical calculations were all performed using GAUSSIAN 16. Geometry optimization and frequency calculations were performed at the B3LYP/6-311 g** level. The structures of all components were optimized through quantum calculation, while restrained electrostatic potential (RESP) atomic charge fitting calculations were performed using MULTIWFN [34] with a scaling factor of 0.7 [35]. The structure-optimized components were mixed proportionally and initial simulation boxes were generated separately using the PACKMOL [36] program, and molecular dynamics simulations were performed using GROMACS 2018.8 [37]. The general AMBER force field (GAFF) was used to describe molecular interactions [38]. All boxes were first energy minimized using the conjugate gradient method, equilibrated in the NPT system for 5 ns at 1000 K and 1 bar temperature and pressure conditions, then NPT simulations were performed for 10 ns at 298 K and 1 bar with compression factors of 0.5 and 2, respectively, and then the current equilibrated box volume was fixed for 20 ns of NVT simulations, and finally, NVT simulations were performed at 298 K for 10 ns for production NVT simulations, and all post-analyses were based on production NVT simulations. The OVITO [39] program was used for structural visualization with export of simulation snapshots. The

compositions of IL-water mixtures for different IL/H₂O ratios in the MD simulations, including the number of IL pairs and water molecules, were included in Table S1.

Log P calculation: The octanol-water partition coefficient (Log P) was generated directly from canonical SMILES strings using RDKit.

IP-EA method: The ECW, the ionization potential (IP) of the anion and the electron affinity (EA) of the cation were calculated by Eqs. ((3)–(5)) [40].

$$ECW = \frac{IP(\text{anion})}{e} - \frac{EA(\text{cation})}{e}, \quad (3)$$

$$IP(\text{anion}) = E(N-1) - E(N), \quad (4)$$

$$EA(\text{cation}) = E(N) - E(N+1), \quad (5)$$

where $E(N)$ is the single point energy of the ion, and $E(N-1)$ and $E(N+1)$ are the single point energies of the ion with one less and one additional electron.

Machine learning model

Conductivity prediction of ILs: Morgan fingerprints with a 2048-vector representation of ILs using RDKit with a radius of 2 nm were computed to serve as high-dimensional feature descriptors for an XGBoost regression model. The dataset comprises 549 room-temperature ionic-liquid conductivity measurements drawn from the ILThermo database [41]. The data were randomly partitioned into training (80%), validation (10%) and test (10%) subsets based on a fixed random seed for reproducibility. Hyperparameter tuning, including the number of trees, learning rate, maximum depth, and subsample ratios, was performed using an XGBoost automated optimization method targeting the minimization of mean squared error on the validation set; early stopping (patience = 50 rounds) was applied to guard against overfitting. The final model deployed on the held-out test set achieved a coefficient of determination $R^2 = 0.71$, a root-mean-square error (MSE) of 1.99 mS/cm and a mean absolute error (MAE) of 0.9 mS/cm [42].

RESULTS AND DISCUSSION

Effect of water content in hydrophilic and hydrophobic ILs to the specific capacity

We conduct a comprehensive investigation combining experimental measurements and computational simulations on five ILs. Previous studies have primarily focused on IL-based supercapacitors sharing the same anion but differing in cations [43]. It is well established that the hydrophilicity or hydrophobicity of the anion plays a crucial role in determining the overall properties of the IL [44]. Therefore, for the five ILs chosen for this study, as shown in Figure 2a, we maintain the same cation 1-ethyl-3-methylimidazolium [C₂mim]⁺ coupled with different anions, including hydrophilic trifluoromethanesulfonate [TFO][−], dicyanofornate [DCA][−], tetrafluoroborate [BF₄][−], hydrophobic bis(fluorosulfonyl)imide [FSI][−] and bis(trifluoromethylsulfonyl)imide [TFSI][−]. The overview of the specific capacitance for the five ILs with different water contents under the same current density is shown in Figure 2b. In hydrophilic ILs, the addition of a moderate amount of water can enhance specific capacitance, despite a concurrent narrowing of the ECW. This highlights a trade-off and suggests that optimizing water content based on IL type is key to maximizing

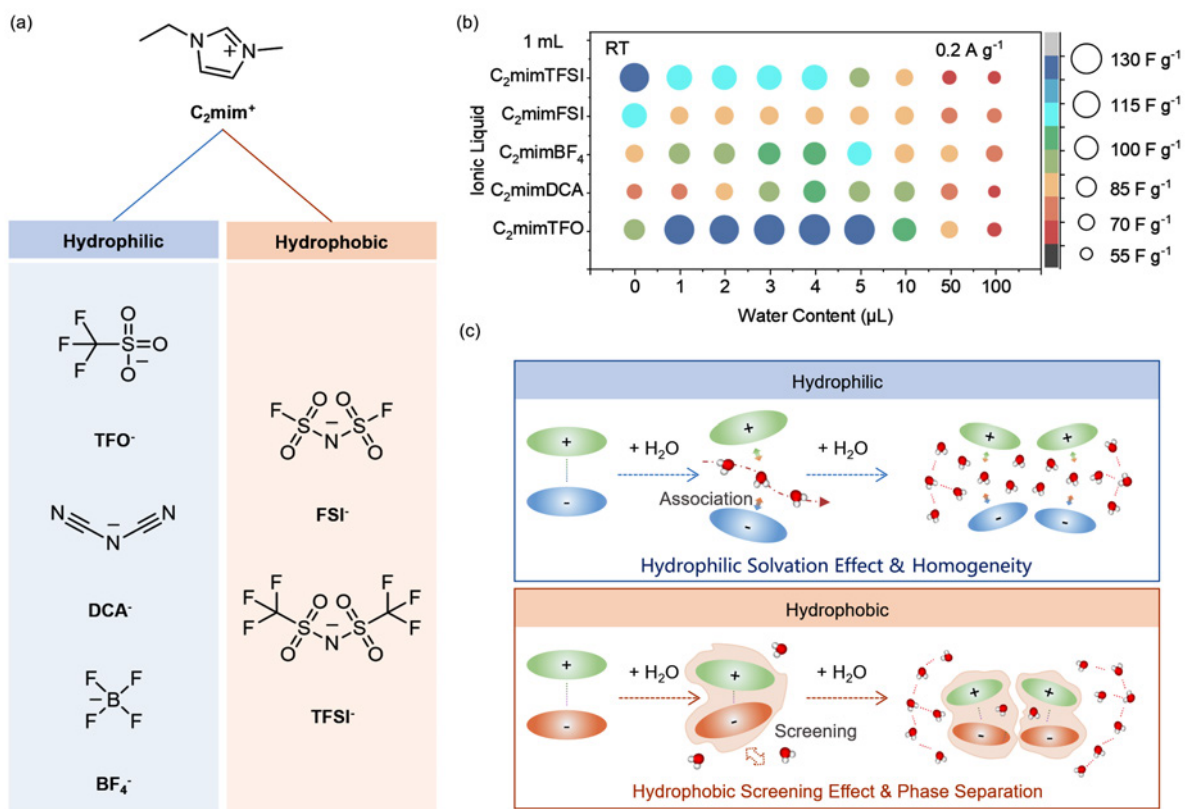


Figure 2 The interaction mechanisms and performance of hydrophilic and hydrophobic ILs with varying water content for supercapacitors. (a) The chemical structures of the five ILs utilized in this study. (b) Heatmap of specific capacitance of the supercapacitors based on the five ILs with varying water contents under a current density of 0.2 A/g. (c) Schematic of water-ion interactions in hydrophilic and hydrophobic ILs.

performance. We demonstrate a mechanism in Figure 2c, which elucidates the diverse impact of the trace water to the hydrophilic and hydrophobic ILs correspondingly. In hydrophilic ILs, the hydrophilic nanocluster and solvation effect promote the interaction between water molecules and IL ions. This interaction disrupts the cation-anion pair, enhancing the accommodation between water molecules and the anions. In contrast, in hydrophobic ILs, the addition of trace amounts of water leads to a tighter nanocluster of cation-anion association, with water molecules being screened from the IL pairs due to limited solvation compatibility. These contrasting interactions between water and ILs with varying hydrophilicity highlight the impact of solvation dynamics and ion associations on the overall performance of IL-water electrolytes for supercapacitors [45]. We further validate and expand the investigation of the interaction dynamics and nano effects through multi-array characterization and theoretical calculations as below.

We compare the room temperature GCD tests for the supercapacitors based on the five ILs and 6 M KOH with activated carbon (AC) electrodes under various current densities in Figure S1. We observe that the ECW of the IL electrolytes is essential to the capacitance of the devices. Pure IL-based supercapacitors exhibit a higher cutoff voltage (2.0–3.5 V) [46] compared to traditional 6 M KOH supercapacitors (1.0 V). Correspondingly, we observe higher specific capacitance of pure IL-based supercapacitors than the 6 M KOH-based supercapacitors, except for $[C_2mim][DCA]$. This is attributed to the insufficient ECW of $[DCA]^-$,

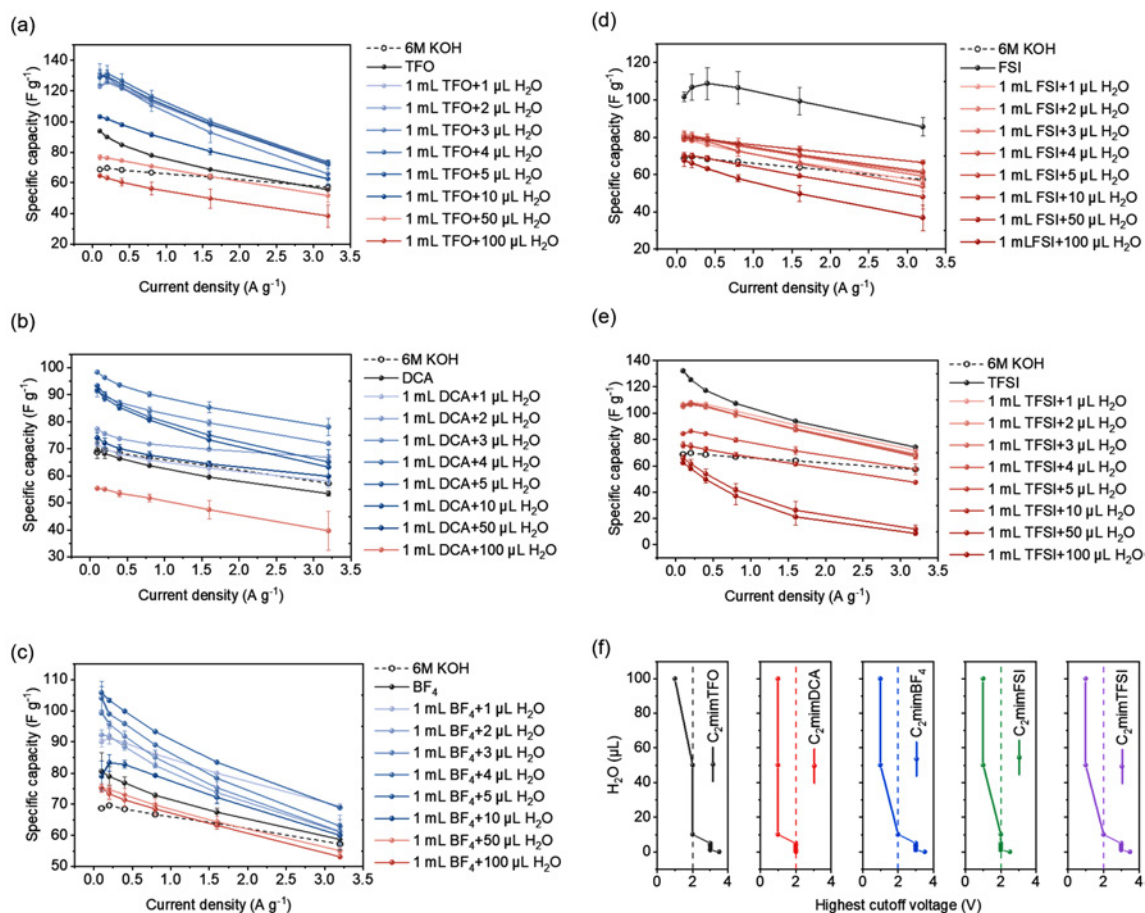


Figure 3 The specific capacitance and highest cutoff voltage of different ILs with varying water contents for supercapacitors. Specific capacitance as a function of water content under different current densities for (a) [C₂mim][TFO], (b) [C₂mim][DCA], (c) [C₂mim][BF₄], (d) [C₂mim][FSI], and (e) [C₂mim][TFSI]. (f) The evolution of the highest cutoff voltage for the IL with varying contents when applied in supercapacitors.

which might originate from the lack of electronegative F atom in [DCA]⁻, whereas all the other anions are fluorine-containing anions, regardless of being hydrophilic or hydrophobic. The higher HOMO of [DCA]⁻ compared to other fluorine-based anions diminishes the electrochemical stability at higher voltages. The quantum calculated HOMO (highest occupied molecular orbital), LUMO, and HOMO-LUMO energy gaps for the five ILs are provided in Table S2.

To investigate the influence of water in the ILs, we prepare a series of supercapacitors with different water contents by increasing the water volume from 0 μL to 100 μL in 1 mL of IL. The specific capacitance of the supercapacitors assembled with hydrophilic and hydrophobic ILs under different water contents is shown in Figure 3a–e. In hydrophilic ILs, including [C₂mim][TFO] [C₂mim][BF₄] and [C₂mim][DCA], the specific capacitance exhibits a peak as a function of water content. A moderate amount of water enhances the specific capacitance, whereas excessive water causes a decrease. To clarify the term “moderate” water content, we define it as the range of water concentration that enhances ionic conductivity while maintaining a sufficiently wide ECW. For [C₂mim][TFO] and [C₂mim][BF₄], the molar ratio of water to IL typically falls between 0.001 and 0.01, while [C₂mim][DCA] can tolerate ratios up to 0.05 without significant loss of performance.

The interaction mechanism between hydrophilic ILs and trace amounts of water in supercapacitors is tunable based on the hydrophilic solvation effect. Specifically, at low water content, the hydrophilic effect disrupts the cation-anion pairs, enhancing ion migration and increasing conductivity, which accelerates ion adsorption onto the electrodes. At higher water levels, water begins to form local nanoclusters, and ultimately the water hydrogen-bond network dominates, causing the mixture to behave as a homogeneous aqueous electrolyte. From the perspective of the electrode interface, hydrophilic ILs encapsulate water molecules, reducing the water adsorption at the electrode-electrolyte interface, which helps maintain stable electrochemical performance [44]. In contrast, hydrophobic IL-based supercapacitors (e.g., [C₂mim][TFSI] and [C₂mim][FSI]) exhibit a simple decrease in specific capacitance as a function of water content. Figure 3f demonstrates that the addition of water reduces the highest cutoff voltage to ~1.0 V for the supercapacitors regardless of hydrophilic or hydrophobic ILs. However, the hydrophobic ILs indicate faster degradation compared to hydrophilic ILs, which might originate from the perturbation of water at the interface with increasing water content, leading to deterioration in capacitance performance and disrupting the order of the electric double-layer at the electrode interface. This ultimately suppresses the ultimate specific capacitance [44,47]. It should be noted that all results in this work are based on AC electrodes. While AC is widely used in supercapacitor research due to its high surface area and porous structure, the observed relationships are specific to the AC-IL system. For instance, Bi *et al.* [44] reported that water addition enhances capacitance in porous carbon but suppresses it on hydrophilic gold due to interfacial water adsorption. Therefore, electrolyte behavior and structure-property trends observed here remain to be further explored in systems involving other electrode materials.

Exploration of the mechanisms of the trace water effect in ILs

We employ a combination of PFG-NMR and conductivity measurements to investigate the influence and underlying mechanisms of trace water on ILs. NMR analysis reveals the impact of trace water on the chemical environment of ILs, as well as its effect on the diffusion coefficients of cations, anions, and water molecules. The ¹H NMR spectra of the five ILs at different water contents are provided in Figure S2. The associated H₂O peaks for the hydrophilic ILs as [C₂mim][TFO], [C₂mim][DCA] and [C₂mim][BF₄] shift towards a lower field and the peak intensity increases significantly with the increasing water content. In contrast, for the hydrophobic ILs as [C₂mim][FSI] and [C₂mim][TFSI], the associated H₂O peaks remain almost unchanged in both position and intensity when the volume ratio of water: IL > 0.05. The ¹H NMR spectra of [C₂mim][FSI] and [C₂mim][TFSI] show free water at 4–5 ppm. This indicates that hydrophobic ILs have low tolerance to water, phase separation occurs macroscopically when the water content exceeds a certain threshold. By integrating the ¹H NMR spectra, the molar ratio of associated H₂O to [C₂mim]⁺ for hydrophilic ILs (Figure 4a) increases linearly with increasing water content, confirming that trace water is indeed incorporated completely into the IL-water mixture. In contrast, for the hydrophobic ILs, when the volume ratio of water: IL exceeds 0.05, the molar ratio of associated H₂O to [C₂mim]⁺ reaches a plateau, indicating that the solubility limit has been reached with excess free water phase separated on top of the NMR tube.

We further employ PFG-NMR to investigate the diffusion properties of water, cations, and anions, thereby revealing the significant impact of water content on ionic mobility. The fitted diffusion coefficients of the

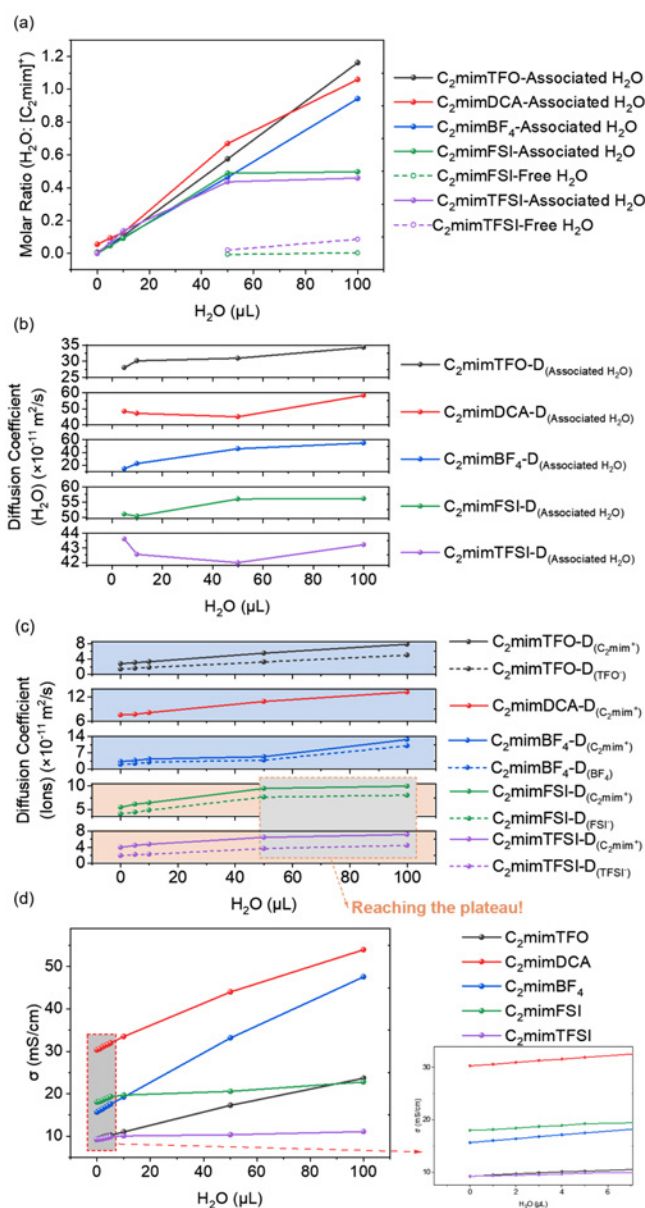


Figure 4 The water content, diffusion coefficients and ionic conductivity for the ILs with varying water contents. (a) The water content based on the integration area of the water peak in ¹H NMR spectra. Diffusion coefficients obtained from PFG-NMR fitting for (b) H₂O and (c) cations and anions. (d) Ionic conductivity of the electrolytes as a function of water content.

associated H₂O, presented in Figure 4b, demonstrate that the diffusion coefficient of associated H₂O for [C₂mim][TFO] and [C₂mim][BF₄] increases monotonically with increasing water content. In contrast, for [C₂mim][DCA], [C₂mim][FSI], and [C₂mim][TFSI], the diffusion coefficient of associated H₂O initially decreases and then increases with water content. The fitted diffusion coefficients of [C₂mim]⁺ and the corresponding anions, as shown in Figure 4c, indicate that in hydrophilic ILs, both cation and anion diffusion coefficients increase synchronously with increasing water content. Similarly, in hydrophobic ILs, the diffusion coefficients of both ionic species increase with the volume ratio of water: IL < 0.05. However, when the volume ratio exceeds 0.05, the diffusion coefficients exhibit no further increase and reach a plateau. This

behavior is consistent with the conductivity results shown in Figure 4d for hydrophobic ILs, where conductivity reaches a plateau with a volume ratio of water: IL > 0.05 . For hydrophobic ILs, conductivity enhancement is suppressed with further water addition. All PFG-NMR spectra are presented in Figures S3–S5.

Evolution of interaction between water and anions in ILs

We conduct molecular dynamics simulations to investigate the role of trace water in ILs. Simulated snapshots of the hydrophilic $[\text{C}_2\text{mim}][\text{TFO}]$ and hydrophobic $[\text{C}_2\text{mim}][\text{TFSI}]$ with varying water contents are shown in Figure 5a. In hydrophilic $[\text{C}_2\text{mim}][\text{TFO}]$, water molecules are well solvated and integrated into the IL network due to strong water-IL interactions. In contrast, in hydrophobic $[\text{C}_2\text{mim}][\text{TFSI}]$, water molecules tend to aggregate into tighter and larger nanoclusters even at low water content, reflecting repulsive interactions between water and hydrophobic ILs. As a result, cations and anions assemble into compact ionic clusters, while water molecules aggregate separately. We also investigate the binding energies of cations and anions, as well as the binding energies between the anions and water through quantum calculations, as shown in Figure S5. The binding energies of $[\text{TFO}]^-$ and $[\text{BF}_4]^-$ with water are < -60 kJ/mol, indicating a stronger ion-water interaction. In contrast, the binding energies of $[\text{FSI}]^-$ and $[\text{TFSI}]^-$ with water are in the range of -40 – -50 kJ/mol, suggesting a relatively looser anion-water interaction compared to the hydrophilic anions. $[\text{DCA}]^-$ shows a binding energy with water that falls between hydrophilic and hydrophobic values, thus explaining the abnormal diffusion behavior of water in $[\text{DCA}]^-$ observed in Figure 4b.

The mean squared displacement (MSD) results from 10 ns simulations exhibit linear trends for water, cations and anions, indicating that the equilibrium state of the simulation box. The diffusion coefficient of water is approximately an order of magnitude higher than that of the cations and anions, which is consistent with the experimental results. In hydrophilic $[\text{C}_2\text{mim}][\text{TFO}]$ (Figure 5b–d), the diffusion coefficient of water increases, indicating that the strong interaction between water and the hydrophilic IL enhances the mobility of water. In hydrophobic $[\text{C}_2\text{mim}][\text{TFSI}]$ (Figure 5e–g), the diffusion coefficient of water initially decreases and then increases, reflecting the complex interaction between water and the hydrophobic anions. These simulation results are highly consistent with the PFG-NMR results.

The radial distribution functions (RDF) of $[\text{C}_2\text{mim}][\text{TFO}]$ and $[\text{C}_2\text{mim}][\text{TFSI}]$ at different water contents, with $[\text{C}_2\text{mim}]^+$ as the center, are shown in Figure 6a, b. We observe that the addition of water disrupts the coordination between $[\text{C}_2\text{mim}]^+$ and $[\text{TFO}]^-$, compared to the pure IL without water. The first peak corresponds to a sharp and strong water peak, and the second peak corresponds to the $[\text{TFO}]^-$ peak. However, in hydrophobic $[\text{C}_2\text{mim}][\text{TFSI}]$, the coordination between $[\text{C}_2\text{mim}]^+$ and $[\text{TFSI}]^-$ still predominates for all water content, demonstrating the existence of the hydrophobic effect and inefficiency of water to break the ion pair in the first coordination nanoshell.

The coordination numbers (CN) of H_2O and anions to the $[\text{C}_2\text{mim}]^+$ (center ion) at different water contents are summarized and compared in Figure 6c, d. Details regarding CN assignments are included in Figure S6. In hydrophilic $[\text{C}_2\text{mim}][\text{TFO}]$, both CNs decrease with increasing water content, which confirms the preferred association between $[\text{TFO}]^-$ and H_2O . The ion clusters become looser with the addition of water, enlarging the ionic transport channels and facilitating ion migration. In hydrophobic $[\text{C}_2\text{mim}][\text{TFSI}]$, the CN of $[\text{C}_2\text{mim}]^+$ with $[\text{TFSI}]^-$ initially exhibits a sharp increase and plateau with increasing water content. This

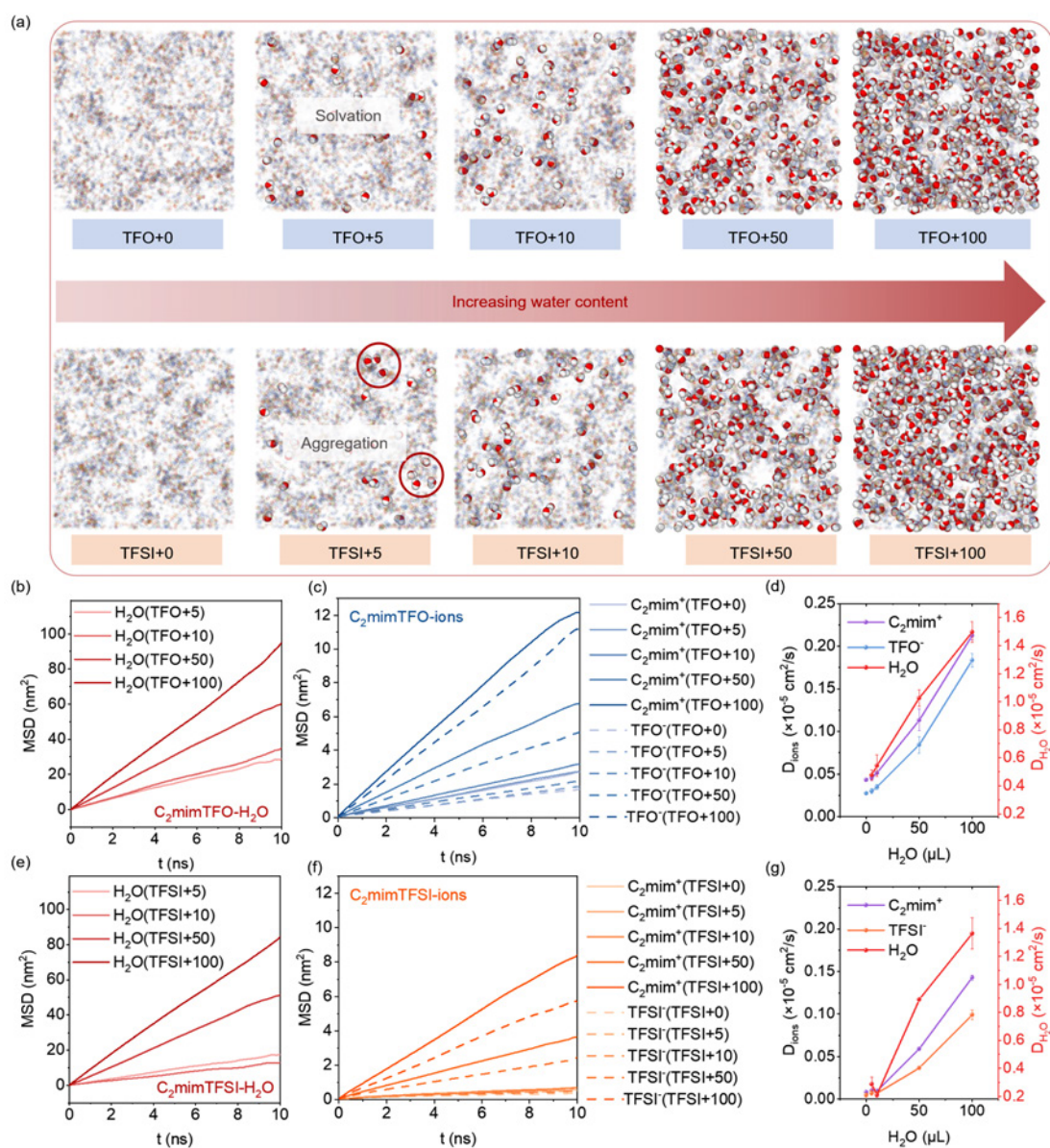


Figure 5 The visualization and diffusion behavior of ILs with water based on molecular dynamics simulations. (a) Molecular dynamics simulation snapshots of [C₂mim][TFO] and [C₂mim][TFSI] at different water contents. MSD of (b) H₂O and (c) cations and anions in the [C₂mim][TFO] at different water contents. (d) Diffusion coefficients of [C₂mim]⁺, [TFO]⁻, and H₂O in the [C₂mim][TFO] at different water contents. MSD of (e) H₂O and (f) cations and anions in the [C₂mim][TFSI] at different water contents. (g) Diffusion coefficients of [C₂mim]⁺, [TFSI]⁻, and H₂O in the [C₂mim][TFSI] at different water contents.

behavior is attributed to the hydrophobic effect at low water concentrations, which causes [TFSI]⁻ to repel water and preferentially coordinate with [C₂mim]⁺, leading to compact ion clusters. The hydrophobic effect maintains a tight association between the cations and anions, and the introduction of small amounts of water fails to significantly disrupt the strong ion pair structure, as shown in hydrophilic ILs. Notably, in [C₂mim][TFSI], the CN of [C₂mim]⁺ with H₂O is < 0.5, which is significantly lower than that in [C₂mim][TFO] (> 3). This further confirms the hydrophobic effect. However, water does promote the overall mobility of the ion clusters, which manifests as a decrease in the viscosity of the electrolyte. Through the molecular dynamic

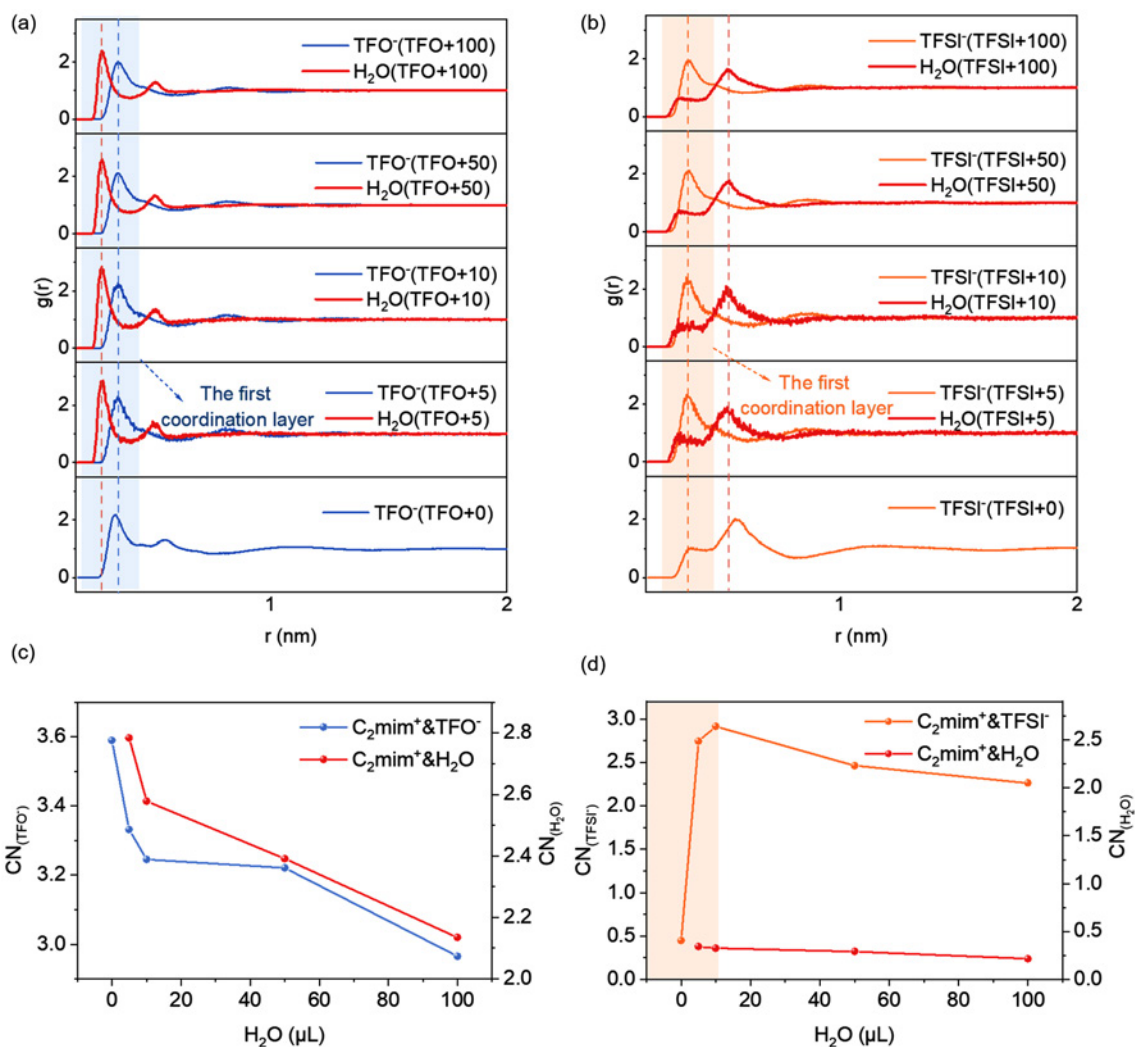


Figure 6 The evolution of radial distribution functions (RDF) and coordination numbers (CN) of (a) [C₂mim][TFO] and (b) [C₂mim][TFSI] centered on [C₂mim]⁺ at different water contents. CN of [C₂mim]⁺ & anions and [C₂mim]⁺ & H₂O in (c) [C₂mim][TFO] and (d) [C₂mim][TFSI] at varying water contents. Calculations are based on the atomcharge.

simulations, we reveal how the variation of water content affects the solvation structure and ion diffusion behavior in ILs, which is highly consistent with experimental observations.

Machine learning-guided inverse design and selection of ILs

Based on experimental validation and computational simulations, we conclude that the two key factors determining the specific capacitance performance of supercapacitors based on ILs are conductivity and ECW. In addition, the effect of water depends strongly on the IL's hydrophilicity. Therefore, we focus on screening pure ILs with favorable conductivity and ECW, while using $\text{Log}P$ as a hydrophilicity descriptor. This framework enables the identification of ILs that are either intrinsically optimal under dry conditions (hydrophobic), or further tunable through water addition (hydrophilic), thus supporting a generalizable

design strategy. To systematically select suitable ILs and accelerate the design process, we employ chemistry-informed machine learning methods to inverse screen the potential candidates for supercapacitors. First, we predict the room-temperature ionic conductivity of the ILs using the XGBoost model. We encode the 2048-dimensional molecular fingerprints of ILs and employ the model to predict the conductivity of the corresponding ILs, thereby establishing the relationship between structure and conductivity. The method is adopted from the recently established Clean Energy Materials Platform (CEMP) in our group, which integrates quantum calculations, experimental data, and predictive models for high-throughput screening of ILs and related materials [7]. The ILs are permutations between $[\text{C}_2\text{mim}]^+$ and 161 anions sourced from ILthermo [41]. The ECW of these 161 ILs is calculated using the IP-EA method [40]. The final evaluation metric (EM) for ILs combines the contributions of both conductivity and ECW with equal contribution as defined in Eq. (6), where the conductivity and ECW are normalized to [0, 1]. A higher value indicates potentially higher specific capacitance of the supercapacitor based on the IL.

$$\text{EM} = 0.5 * \text{conductivity} + 0.5 * \text{ECW}. \quad (6)$$

The hydrophilicity and hydrophobicity of all ILs are further assessed using the $\text{Log}P$ parameter in Figure 7a. According to the experimental results, we propose that hydrophilicity is essential to the final performance of IL-based supercapacitors; thus, we employ the hydrophobic benchmark $[\text{C}_2\text{mim}][\text{TFSI}]$, which has a $\text{Log}P$ of 1.3918, as the threshold. ILs with $\text{Log}P < 1.3918$ are classified as hydrophilic, while those with $\text{Log}P > 1.3918$ are hydrophobic. Using this criterion, 62 hydrophobic ILs and 99 hydrophilic ILs are selected. Furthermore, we impose a threshold of $\text{ECW} > 2.5 \text{ V}$ for the ILs and exclude the five ILs discussed in this study. After applying these filters, the remaining hydrophobic ILs are evaluated in terms of conductivity and ECW (Figure 7b), and the top 10 candidates with the highest EM values are selected (Figure 7c); their anion structures are displayed in Figures 7d. Additionally, we found that hydrophobic anions with higher fluorine content and larger molecular steric hindrance generally exhibit better performance due to more stable ions, which positively affect the expansion of ECW. Similarly, the conductivity and ECW performance of the hydrophilic ILs are compared in Figure 7e. The hydrophilic ILs with the top 10 EM and corresponding anion structures are summarized in Figure 7f, g. We observe that hydrophilic anions with water-attracting elements (such as N or O) generally exhibit smaller steric hindrance compared to hydrophobic ILs, leading to a significant improvement in conductivity. Furthermore, we believe that adding trace amounts of water to hydrophilic ILs can further enhance the specific capacitance of the supercapacitors.

We further interpret the XGBoost model to extract the impact of the chemical structure of ILs on conductivity. Figure 8a illustrates the inverse design process by utilizing inverse decoding of the hashed Morgan molecular fingerprints and SHAP analysis. Then, through SHAP analysis of the top 20 features of the XGBoost model (Figure 8b), we further identify the positive and negative impacts of various features in the molecular fingerprints on conductivity. Based on this, we obtain molecular fingerprint mapping information for features that positively and negatively impact conductivity, as shown in Figure 8c. We find that specific cationic groups (such as those containing an imidazole ring) and anionic groups (such as those with trifluoromethyl or nitrogen anions) help enhance the conductivity of ILs, while certain cationic groups (such as those with triangular rings or quaternary ammonium cations) and anionic groups (such as those with long carbon chains, oxygen anions, or carbonyl groups) may diminish conductivity. These findings provide direct structural guidance for designing ILs with high conductivity, facilitating the subsequent design and synthesis

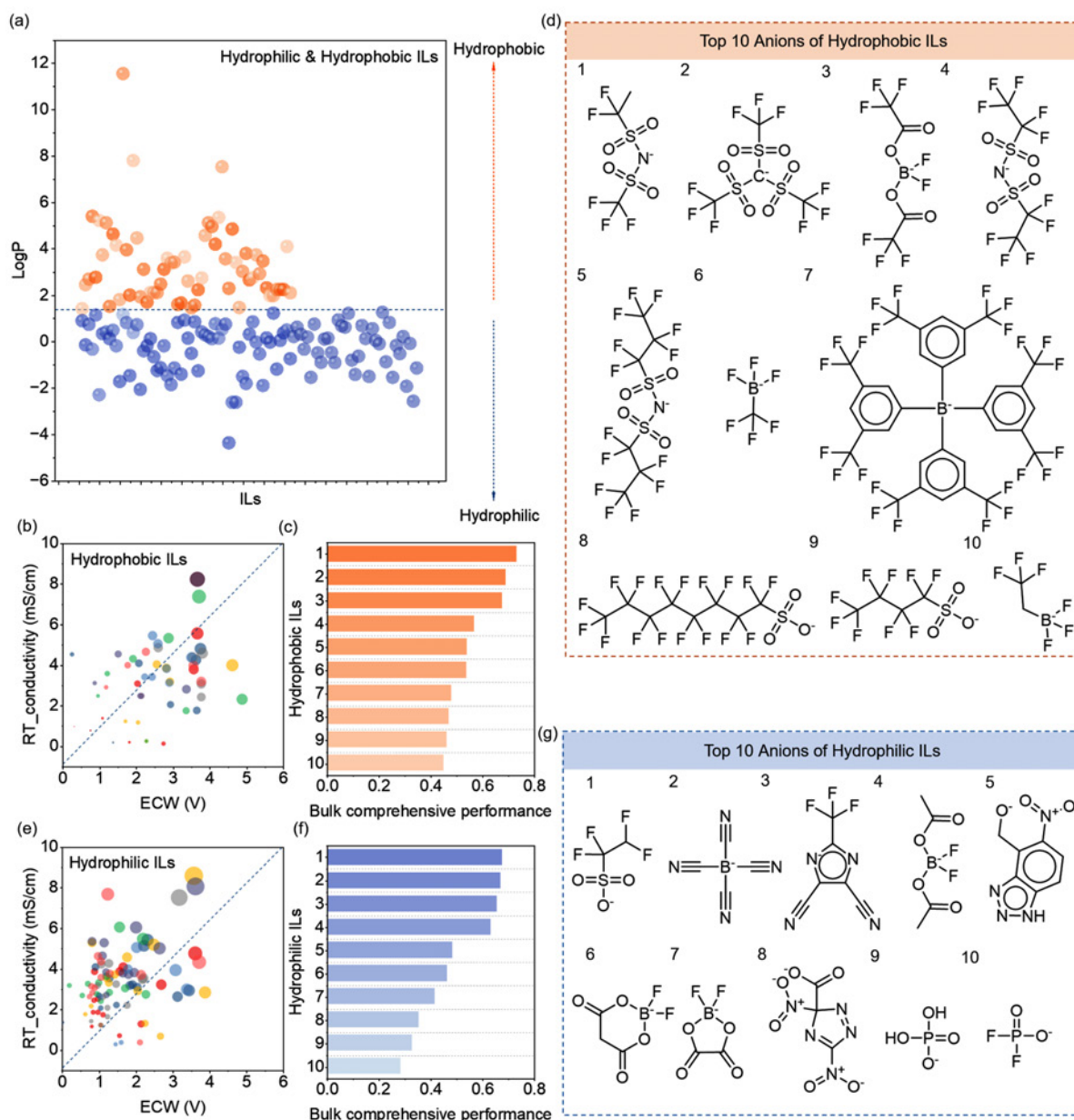


Figure 7 Machine learning-guided screening of ILs for supercapacitors. (a) The calculated LogP values of all ILs with [C₂mim]⁺ as the cation and 161 anions sourced from ILthermo. (b) Comparison of the predicted ionic conductivity and calculated ECW for all hydrophobic ILs with [C₂mim]⁺ as the cation and 161 anions sourced from ILthermo. (c) Comparison of evaluation metric among the top 10 hydrophobic ILs and (d) their respective anion structures. (e) Comparison of the predicted ionic conductivity and calculated ECW of all hydrophilic ILs with [C₂mim]⁺ as the cation and 161 anions sourced from ILthermo. (f) Comparison of evaluation metric among the top 10 hydrophilic ILs and (g) their respective anion structures.

of high-performance ILs. Despite the reasonably high accuracy ($R^2 = 0.71$), the current model has several limitations. First, the dataset size remains modest, which may constrain generalizability. Second, while tree-based models such as XGBoost offer some interpretability, they do not directly capture long-range molecular interactions or temperature effects, which may also influence conductivity. Expanding the dataset and incorporating physics-aware descriptors could further enhance predictive power and robustness.

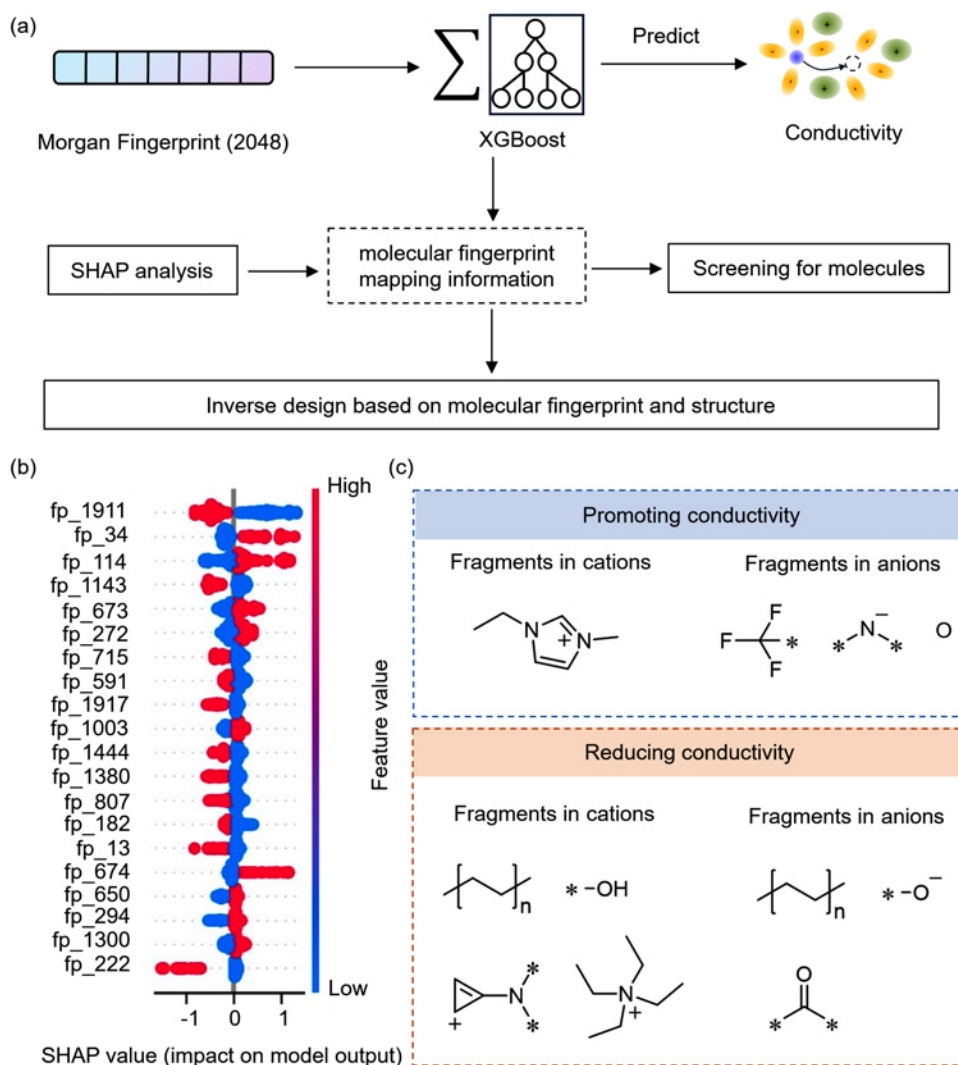


Figure 8 Machine learning-guided inverse design of IL structures. (a) The inverse design process of ILs based on Morgan molecular fingerprints and SHAP analysis. (b) The top 20 most important features in the global SHAP summary plot. (c) Inverse design of cation and anion fragments based on molecular fingerprints and structure, with respective positive and negative influences on conductivity.

CONCLUSION

We conclude that water plays a critical role in both hydrophilic and hydrophobic ILs as applied in supercapacitors. In hydrophilic ILs, water molecules compete with anions for coordination with cations via the hydrophilic effect, weakening the coordination between cations and hydrophilic anions, thus accelerating ion diffusion with enhanced specific capacitance. In hydrophobic ILs, water molecules enhance cation–anion coordination via the hydrophobic screening effect, meanwhile disturbing the electrolyte–electrode interfaces, displaying a diminished performance. Beyond the chemical insights of the mechanics, we implement a machine learning-assisted inverse design strategy that combines ECW (IP-EA calculations) with predicted ionic conductivity (XGBoost) for generated ILs with the same cation and 161 anions with varying hydrophilicity. By incorporating hydrophilicity based on calculated $\text{Log}P$ values of the anions, the inverse

screening framework enables efficient selection of IL candidates with optimal performance trade-offs. We further utilize Morgan molecular fingerprints and SHAP analysis to reveal the impact of structure fingerprint on conductivity and perform inverse design of the cations and anions. This integrated experimental data-driven approach provides a robust pathway for accelerating the discovery and rational design of next-generation materials for energy storage and conversion devices.

Data availability

The original data are available from corresponding authors upon reasonable request.

Acknowledgements

The computations in this research were performed using the CFFF platform of Fudan University.

Funding

This work was supported by the National Natural Science Foundation of China (92372126, 52373203), the Excellent Young Scientists Fund Program, and the AI for Science Foundation of Fudan University (FudanX24AI014).

Author contributions

Q.C. performed all the experiments and analyzed the data. J.W. was responsible for theoretical calculations and artificial intelligence. Q.C. wrote the manuscript and Y.W. conceived the idea and revised the manuscript.

Conflict of interest

The authors declare no conflict of interest.

Supplementary information

The supporting information is available online at <https://doi.org/10.1360/nso/20250025>. The supporting materials are published as submitted, without typesetting or editing. The responsibility for scientific accuracy and content remains entirely with the authors.

References

- 1 Khan HA, Tawalbeh M, Aljawmeh B, *et al.* A comprehensive review on supercapacitors: Their promise to flexibility, high temperature, materials, design, and challenges. *Energy* 2024; **295**: 131043.
- 2 Chang JK, Lee MT, Tsai WT, *et al.* X-ray photoelectron spectroscopy and *in situ* X-ray absorption spectroscopy studies on reversible insertion/desertion of dicyanamide anions into/from manganese oxide in ionic liquid. *Chem Mater* 2009; **21**: 2688–2695.
- 3 Dou Q, Liu L, Yang B, *et al.* Silica-grafted ionic liquids for revealing the respective charging behaviors of cations and anions in supercapacitors. *Nat Commun* 2017; **8**: 2188.
- 4 Lundin F, Stettner T, Falus P, *et al.* Effect of water on local structure and dynamics in a protic ionic liquid-based electrolyte. *ChemSusChem* 2025; **18**: e202402753.
- 5 Matuszek K, Piper SL, Brzeczek-Szafran A, *et al.* Unexpected energy applications of ionic liquids. *Adv Mater* 2024; **36**: 2313023.
- 6 Yao N, Chen X, Fu ZH, *et al.* Applying classical, *ab initio*, and machine-learning molecular dynamics simulations to the liquid electrolyte for rechargeable batteries. *Chem Rev* 2022; **122**: 10970–11021.
- 7 Wang J, Ju J, Wang Y. CEMP: A platform unifying high-throughput online calculation, databases and predictive models

- for clean energy materials. 2025, arXiv: 2507.04423.
- 8 Racki A, Padászyński K. Recent advances in the modeling of ionic liquids using artificial neural networks. *J Chem Inf Model* 2025; **65**: 3161–3175.
 - 9 Xiao P, Yun X, Chen Y, *et al.* Insights into the solvation chemistry in liquid electrolytes for lithium-based rechargeable batteries. *Chem Soc Rev* 2023; **52**: 5255–5316.
 - 10 Manna SS, Manna S, Pathak B. Molecular dynamics-machine learning approaches for the accurate prediction of electrochemical windows of ionic liquid electrolytes for dual-ion batteries. *J Mater Chem A* 2023; **11**: 21702–21712.
 - 11 Yang Y, Yao N, Gao Y, *et al.* Data-knowledge-dual-driven electrolyte design for fast-charging lithium ion batteries. *Angew Chem Int Ed* 2025; **64**: e202505212.
 - 12 Gao YC, Yao N, Chen X, *et al.* Data-driven insight into the reductive stability of ion-solvent complexes in lithium battery electrolytes. *J Am Chem Soc* 2023; **145**: 23764–23770.
 - 13 Xue CF, Wang L, Yang LX, *et al.* Nitrogen self-doped biochar sustainably self-activated from cactus solidified with freeze-drying strategy for lightweight supercapacitor. *ACS Sustain Chem Eng* 2024; **12**: 15961–15971.
 - 14 Qing L, Jiang J. Enabling high-capacitance supercapacitors by polyelectrolyte brushes. *ACS Nano* 2023; **17**: 17122–17130.
 - 15 Qi J, Bao K, Wang W, *et al.* Emerging two-dimensional materials for proton-based energy storage. *ACS Nano* 2024; acsnano.4c06737.
 - 16 Cui S, Miao W, Wang X, *et al.* Multifunctional zincophilic hydrogel electrolyte with abundant hydrogen bonds for zinc-ion capacitors and supercapacitors. *ACS Nano* 2024; **18**: 12355–12366.
 - 17 Kang YJ, Yoo Y, Kim W. 3-V solid-state flexible supercapacitors with ionic-liquid-based polymer gel electrolyte for AC line filtering. *ACS Appl Mater Interfaces* 2016; **8**: 13909–13917.
 - 18 Gao R, Song Y, Ye Q, *et al.* Double-cross-linked and stretchable ionogels with tunable mechanics and ionic conductivity for thermal and mechanical sensors. *ACS Appl Mater Interfaces* 2025; **17**: 20296–20306.
 - 19 Halder J, De P, Chandra A. Synergistic contribution of redox additive electrolytes to significantly increase the performances of hybrid supercapacitors. *J Energy Storage* 2024; **104**: 114583.
 - 20 Benjamin M, Manoj D, Karnan M, *et al.* Switching the solubility of electroactive ionic liquids for designing high energy supercapacitor and low potential biosensor. *J Colloid Interface Sci* 2021; **588**: 221–231.
 - 21 Wang J, Buzolic JJ, Mullen JW, *et al.* Nanostructure of locally concentrated ionic liquids in the bulk and at graphite and gold electrodes. *ACS Nano* 2023; **17**: 21567–21584.
 - 22 Park JH, Rana HH, Kim JS, *et al.* Inorganic-organic double network ionogels based on silica nanoparticles for high-temperature flexible supercapacitors. *ACS Appl Mater Interfaces* 2023; **15**: 37344–37353.
 - 23 Yang Y, Liu M, Zhang D, *et al.* “Water in ionic liquid” electrolyte toward supercapacitors with high operation voltage, long lifespan, and wide temperature compatibility. *Battery Energy* 2025; **4**: e20240089.
 - 24 Zhao Z, Huang Y, Zheng H, *et al.* Cotton fiber/PVA-based neutral hydrogel with Al³⁺ as an electrolyte additive for high-performance supercapacitors. *ACS Appl Energy Mater* 2023; **6**: 644–656.
 - 25 Feng G, Jiang X, Qiao R, *et al.* Water in ionic liquids at electrified interfaces: The anatomy of electrosorption. *ACS Nano* 2014; **8**: 11685–11694.
 - 26 Xie J, Lin D, Lei H, *et al.* Electrolyte and interphase engineering of aqueous batteries beyond “water-in-salt” strategy. *Adv Mater* 2024; **36**: 2306508.
 - 27 Khan Z, Martinelli A, Franco LR, *et al.* Mass transport in “water-in-polymer salt” electrolytes. *Chem Mater* 2023; **35**: 6382–6395.
 - 28 Park J, Lee J, Kim W. Redox-active water-in-salt electrolyte for high-energy-density supercapacitors. *ACS Energy Lett* 2022; **7**: 1266–1273.
 - 29 Yu J, Yu C, Song X, *et al.* Microscopic-level insights into solvation chemistry for nonsolvating diluents enabling high-voltage/rate aqueous supercapacitors. *J Am Chem Soc* 2023; **145**: 13828–13838.
 - 30 Feng G, Jiang X, Qiao R, *et al.* Water in ionic liquids at electrified interfaces: The anatomy of electrosorption. *ACS*

- Nano* 2014; **8**: 11685–11694.
- 31 Elfgen R, Gehrke S, Hollóczki O. Ionic liquids as extractants for nanoplastics. *ChemSusChem* 2020; **13**: 5449–5459.
- 32 Song Y, Ju J, Wang J, *et al.* Multi-objective optimization of ionic polymer electrolytes for high-voltage fast-charging and versatile lithium batteries. *Adv Mater* 2025; **37**: 2500941.
- 33 Zhang C, Jin Z, Zeng B, *et al.* Characterizing the brownian diffusion of nanocolloids and molecular solutions: Diffusion-ordered NMR spectroscopy vs dynamic light scattering. *J Phys Chem B* 2020; **124**: 4631–4650.
- 34 Lu T, Chen F. Multiwfn: A multifunctional wavefunction analyzer. *J Comput Chem* 2012; **33**: 580–592.
- 35 Bayly CI, Cieplak P, Cornell W, *et al.* A well-behaved electrostatic potential based method using charge restraints for deriving atomic charges: The RESP model. *J Phys Chem* 1993; **97**: 10269–10280.
- 36 Martínez L, Andrade R, Birgin EG, *et al.* Packmol: A package for building initial configurations for molecular dynamics simulations. *J Comput Chem* 2009; **30**: 2157–2164.
- 37 Hess B, Kutzner C, van der Spoel D, *et al.* Gromacs 4: Algorithms for highly efficient, load-balanced, and scalable molecular simulation. *J Chem Theor Comput* 2008; **4**: 435–447.
- 38 Wang J, Wolf RM, Caldwell JW, *et al.* Development and testing of a general amber force field. *J Comput Chem* 2004; **25**: 1157–1174.
- 39 Stukowski A. Visualization and analysis of atomistic simulation data with OVITO—the open visualization tool. *Model Simul Mater Sci Eng* 2010; **18**: 015012.
- 40 Wang J, Wang Y. Strategies to improve the quantum computation accuracy for electrochemical windows of ionic liquids. *J Phys Chem B* 2024; **128**: 1943–1952.
- 41 Dong Q, Muzny CD, Kazakov A, *et al.* ILThermo: A free-access web database for thermodynamic properties of ionic liquids. *J Chem Eng Data* 2007; **52**: 1151–1159.
- 42 Li K, Wang J, Song Y, *et al.* Machine learning-guided discovery of ionic polymer electrolytes for lithium metal batteries. *Nat Commun* 2023; **14**: 2789.
- 43 Ahmed M, Tatrari G, Johansson P, *et al.* Sweet ionic liquids as high-temperature and high-voltage supercapacitor electrolytes. *ACS Sustain Chem Eng* 2024; **12**: 16896–16904.
- 44 Bi S, Wang R, Liu S, *et al.* Minimizing the electrosorption of water from humid ionic liquids on electrodes. *Nat Commun* 2018; **9**: 5222.
- 45 Zheng Q, Goodwin ZAH, Gopalakrishnan V, *et al.* Water in the electrical double layer of ionic liquids on graphene. *ACS Nano* 2023; **17**: 9347–9360.
- 46 Kim TY, Lee HW, Stoller M, *et al.* High-performance supercapacitors based on poly(ionic liquid)-modified graphene electrodes. *ACS Nano* 2011; **5**: 436–442.
- 47 Fajardo OY, Bresme F, Kornyshev AA, *et al.* Water in ionic liquid lubricants: Friend and foe. *ACS Nano* 2017; **11**: 6825–6831.